



Development, characterization and mechanisms study of protonated sawdust biochar-chitosan composite bead biosorbent for defluoridation of contaminated groundwater

Nadu Kankanamge Lahiru Chathushan Rupasinghe, Senanayake Mudiyansele Aroshi Erandika Senanayake, K.G.N. Nanayakkara*

Department of Civil Engineering, Faculty of Engineering, University of Peradeniya, 20400, Sri Lanka

ARTICLE INFO

Keywords:
Adsorption
Biosorbent
Chitosan
Defluoridation
Protonation

ABSTRACT

Protonated Sawdust Biochar Chitosan Composite Bead (PSCCB) biosorbent was prepared to compare its defluoridation capacity against raw chitosan from synthetic fluoride solution. Chitosan sawdust biochar beads were chemically modified via crosslinking and protonation to utilize amine and hydroxyl functional groups to enhance defluoridation. Adsorbents were characterized by BET, SEM, XRD, FTIR and zero point charge analysis. High pore volume of PSCCB yielded higher surface area of 57.97 m²/g after modification. Batch experiments revealed that PSCCB has an excellent defluoridation capacity of more than 90% at pH 7 within an equilibrium time of 60 min. Experimental data of PSCCB fitted well with Langmuir isotherm model and followed pseudo second order kinetic model. The maximum monolayer adsorption capacity of PSCCB was 4.413 mg/g. The dominant mechanism of fluoride removal was proposed as formation of hydrogen bonds with protonated amines in PSCCB. Field trials were conducted on groundwater samples collected from three distinct locations.

1. Introduction

Groundwater has become the main drinking water source in many countries and reportedly provides drinking water for at least 50% of the world's population (Connor, 2015). Fluoride is among the major contaminants found in groundwater and depending on its concentration it could be beneficial or detrimental to health. Hence, the World Health Organization (WHO) has set an upper limit of fluoride content in drinking water as 1.5 mg/l. Furthermore, it has been reduced to 1 mg/l in tropical countries. Chronic intake of water containing high levels of fluoride could lead to several health issues such as dental fluorosis, skeletal fluorosis, and kidney diseases (Dissanayake, 2010; Wu et al., 2021). In addition to this, it may even cause neurological abnormalities along with structural and functional damages to several organs in humans. Several studies have conducted in depth research on fluoride toxicity in human health and also elaborate the economic consequences in this regard (Banerjee et al., 2021; Kut et al., 2016). While affecting the potability of drinking water, the enrichment of fluoride in irrigation water and soil has been found to be detrimental to food crops as well (Banerjee et al., 2021; Struneka and Struncky, 2020; Zhang et al.,

2018). A wide range of methods has been implemented to remove fluoride in water, including chemical precipitation, ion exchange, reverse osmosis, nano-filtration, and electrodialysis. However, adsorption has gained the spotlight due to its effectiveness and low cost (Wu et al., 2020).

A wide range of adsorbents and their modifications have been employed for the removal of fluoride from water. These include oxides and hydroxides, geomaterials, carbonaceous materials, industrial products, and by-products and biosorbents (Habuda-Stanić et al., 2014). Studies conducted for the past decade provide evidence that biosorption is a promising technique to remove fluoride from water. Among biosorbents, chitosan holds a special place since it offers several advantages over other adsorbents due to its low cost, environmental friendliness, hydrophilic nature and natural abundance (Ayub et al., 2020; Lee et al., 2009). The effectiveness of chitosan and its modifications in the removal of fluoride have been extensively studied for the past decade (Waghmare et al., 2015). The presence of amine and hydroxyl functional groups of chitosan allows it to be physically and chemically modified via cross-linking, grafting, chelating with metal ions, and also by forming into beads. Chitosan has also been combined with other materials to form

* Corresponding author.

E-mail addresses: nadeen@eng.pdn.ac.lk, kgnn@pdn.ac.lk (K.G.N. Nanayakkara).

composites to further enhance its defluoridation capacity (Korde et al., 2020; Kusriani et al., 2019).

Biochar possesses a porous structure similar to activated carbon and has been used as an adsorbent to remove various pollutants in water (Dai et al., 2019; Li et al., 2020). Biochar exhibits superior qualities as an adsorbent due to the presence of a large number of oxygen containing surface functional groups, high specific surface area, and high porosity (Liang et al., 2021; Tomczyk et al., 2020). The application of biochar in environmental remediation has been studied extensively in terms of heavy metals and organic pollutants removal (Dai et al., 2019; Liu et al., 2021). Furthermore, recent studies have also proven the applicability of biochar based catalysts in the photocatalytic degradation of organic pollutants owing to the high stability of biochar (Qiu et al., 2021). Biochar is environmentally friendly and could be produced through simple pyrolysis, at a low cost. Sawdust is one of the sources of biochar produced in large quantities at sawmills. Sawdust biochar could be prepared by pyrolyzing sawdust at elevated temperatures in an oxygen-depleted environment (Mohan et al., 2014). Recent studies show the potential of sawdust biochar in the removal of various pollutants in drinking water including fluoride (Guan et al., 2015; Zhou et al., 2017).

Few shortcomings of chitosan as an adsorbent include low porosity, surface area, and low pore volume. This study explores the adsorption capacity of chitosan on removing fluoride in synergistic nature with sawdust biochar by overcoming the aforementioned drawbacks. Adsorbents, in general, tend to display weak adsorption capacity at low fluoride concentrations, hence; this study also focuses on investigating the efficacy of PSCCB at low fluoride levels, which has been overlooked in previous research using biosorbents. Moreover, a myriad of research has been conducted to enhance the defluoridation capacity of biosorbents by incorporating multivalent metal ions having a high affinity towards fluoride which could be costly, but this study aims to produce a novel biosorbent that is comparatively low cost, eco-friendly, biodegradable, bio-compatible, and possessing high adsorption capacity. Chitosan biochar composite beads were suitably modified via cross-linking followed by protonation to further enhance its defluoridation capacity. A comparative adsorption efficiency study on raw chitosan and PSCCB was made using batch experiments. The effect of various influencing parameters such as contact time, initial fluoride concentration, and adsorbent dosage on adsorption efficiency was evaluated. Furthermore, adsorption isotherm and kinetic studies were conducted and finally, the applicability of the adsorbent in actual groundwater samples was evaluated.

2. Materials and methods

2.1. Materials

Chitosan powder was obtained from Norwegian University of Life Sciences and was used as the raw material without any modification. Physical modification of chitosan was carried out using glacial acetic acid (CH_3COOH), sodium hydroxide (NaOH), and pyrolyzed biochar prepared from softwood sawdust ($550\text{ }^\circ\text{C}$ – $660\text{ }^\circ\text{C}$). Anhydrous sodium fluoride (NaF) was used to prepare the synthetic fluoride solution. Crosslinking of chitosan beads was carried out using Glutaraldehyde solution (Grade II, 25% in H_2O). Concentrated hydrochloric acid (HCl) was used for the protonation of the beads. HACH fluoride SPADNS reagent with a fluoride detection range of 0–2 mg/l was used to measure the fluoride concentration. All the chemicals and reagents used were of analytical grade. The actual ground water samples were collected from three fluoride rich Reverse Osmosis plants in Sri Lanka for the field study,

2.2. Preparation of sawdust-biochar

Sawdust biochar was prepared by pyrolyzing softwood sawdust collected from a local sawmill. A continuous type Down Draft Double

Chamber slow pyrolysis reactor was used for pyrolyzing sawdust, maintaining the temperature range of $550\text{ }^\circ\text{C}$ – $660\text{ }^\circ\text{C}$ and a residence time of 40 min. As per reported literature, pore volume and surface area show an increasing trend with the increase in pyrolysis temperature and decrease along with the disappearance of $-\text{OH}$ containing functional groups at very high temperatures ($>700\text{ }^\circ\text{C}$), (Cheng et al., 2021; Li et al., 2017). Hence, a mid temperature range for pyrolysis was used for optimum defluoridation. The resulting biochar was washed several times with distilled water to remove any adhered impurities and oven-dried for 24 h at $37\text{ }^\circ\text{C}$. The dried biochar was then grounded and sieved through a 75-micron sieve and used for adsorption studies without further modification.

2.3. Preparation of chitosan-biochar composite beads

Initially, the chitosan solution was prepared by dissolving 1 g of chitosan powder into 100 ml of 1.0% (v/v) acetic acid solution. Then, 1 g of sawdust biochar powder was added to the chitosan solution and stirred using a magnetic stirrer for 3 h at room temperature. After mixing, the solution was added drop wise to 1.0 M Sodium Hydroxide solution through a syringe, at a constant rate to prepare composite beads. The beads were kept in the NaOH solution for 24 h. Finally, chitosan-biochar composite beads were washed several times, until reaching constant wash water pH, with distilled water to remove excess NaOH .

2.4. Preparation of protonated sawdust chitosan composite beads

The wet sawdust chitosan composite beads were cross-linked with 2.5 wt% glutaraldehyde solution (glutaraldehyde solution:wet chitosan beads = 10 ml:1 g). The mixture was kept in a refrigerator at $25\text{ }^\circ\text{C}$ for 48 h to facilitate cross-linking reaction. The cross-linked beads were washed with distilled water to remove any free glutaraldehyde. Thereafter, the beads were treated with concentrated HCl for about 30 min for protonation of amine groups in chitosan (Viswanathan et al., 2009a). The resulting Protonated Sawdust Chitosan Composite Beads (PSCCB) were then washed with distilled water to a constant pH, dried at room temperature and used for adsorption studies.

2.5. Characterization of raw and modified adsorbents

Change in the crystalline structures and the mineral composition of the raw chitosan and PSCCB analyzed using X-ray Diffraction (XRD) Analysis. The XRD spectra both adsorbents were obtained in the 2θ range from 5° to 80° using Bruker D8 Advanced Eco Powder X-ray Diffractometer. To identify the change in surface morphology and microstructure Scanning Electron Microscopy (SEM) images were taken at the high and low magnification levels. Electron Dispersive X-ray (EDX) analysis was used to identify the change in surface chemical compositions. Both SEM and EDX analyses were conducted using Hitachi SU6600 Scanning Electron Microscope. The functional groups in the raw chitosan powder and PSCCB were identified by analyzing the peak frequencies in FTIR spectra, obtained in transmittance mode using a PerkinElmer Spectrum Two FT-IR Spectrometer equipped with ATR reflectance cell. Specific surface area of adsorbents was determined using the Brunauer, Emmet, and Teller (BET) method by N_2 adsorption at 77 K using Quantachrome Autosorb iQ Surface Area Analyzer. The surface area is reported using the BET method whereas the pore volume and the pore radius is reported using the Barret Joyner Halenda (BJH) method analyzed by the same instrument. The pH at which the surface charge of the material is zero in the aqueous media or in other words the pH point of zero charge (pH_{zpc}) of the adsorbent materials was determined using pH drift method.

2.6. Adsorption experiments

2.6.1. Synthetic fluoride experiments

A stock solution (100 mg/l) of fluoride was prepared by dissolving anhydrous sodium fluoride in deionized water. The stock solution was diluted to obtain the desired concentration of fluoride for adsorption experiments. Batch experiments were conducted to study the effect of various influencing parameters such as contact time, adsorbent dosage and initial fluoride concentration. All experiments were conducted at room temperature (25 °C) and neutral pH was maintained throughout the experiments since the groundwater pH is closer to the neutral pH. Samples were shaken in a mechanical shaker at 200 rpm in each experiment. Sorption experiments conducted with raw chitosan were filtered using Whatman No. 42 filter paper and filtrate was analyzed for fluoride concentration by SPANDS method using a portable colorimeter.

2.6.2. Actual Groundwater experiments

The fluoride removal efficiency of PSCCB was tested in actual groundwater samples collected from three distinct locations from Anuradhapura and Polonnaruwa districts in Sri Lanka. The water quality parameters of the three samples are given in Table 1. The fluoride sorption tests were conducted at 25 °C with a 5 g/l adsorbent dosage for 60 min.

3. Results and discussion

3.1. Characterization

3.1.1. X-ray diffraction (XRD) analysis

X-ray diffraction patterns of both raw chitosan powder and PSCCB are given in supplementary material. The two typical characteristic crystallization peaks of raw chitosan appear at $2\theta = 10.6^\circ$ and $2\theta = 19.9^\circ$ with an intensity of 2244 at $2\theta = 19.9^\circ$, followed by two sharp reflections at $2\theta = 26.6^\circ$ and $2\theta = 29.5^\circ$ with much lower intensities in the XRD spectra (Hu et al., 2013; Kolhe and Kannan, 2003; Zhang et al., 2019). In PSCCB, the reflection around $2\theta = 10^\circ$ has disappeared and the strong $2\theta = 19.9^\circ$ reflection has diminished and shifted. There is a broader peak centering at around $2\theta = 23^\circ$ followed by a relatively sharp reflection at $2\theta = 26.9^\circ$ with an intensity of 719. It could be noted that the intensity of the peak is much lower than that of the native chitosan. This indicates that there is a significant decrease in crystallinity of chitosan upon forming PSCCB. This implies that the presence of sawdust biochar and the crosslinking reaction with subsequent treatment with HCl has destroyed the original configuration of chitosan by heavily disturbing the regularity among chitosan polymer chains. (Hu et al., 2013; Zhang et al., 2019). It could be concluded that PSCCB is more amorphous in nature and allows better accessibility to fluoride in adsorption.

Table 1
Water quality parameters of groundwater samples.

Water quality parameters	Location 1 (Medirigiriya) 8.101279° N 80.950261° E	Location 2 (Kahatagasdigiya) 8.441461° N 80.661923° E	Location 3 (Thambuthagama) 8.184715° N 80.310184° E
Initial F ⁻ (mg/l)	0.60	3.30	0.50
EC (µs/cm)	350.4	127.4	313.7
TDS (ppm)	172.2	624.8	154.2
Ca ²⁺ (ppm)	19.47	7.49	13.48
Mg ²⁺ (ppm)	31.17	67.78	23.99
Hardness (ppm)	176.97	297.82	132.45
Na ⁺ (ppm)	90.09	506.34	90.79

3.1.2. Scanning electron microscopy — electron dispersive X-ray (SEM-EDX) analysis

SEM images of raw chitosan powder and modified chitosan beads taken at low and high magnification levels are shown in Fig. 1. The SEM image of raw adsorbent (Fig. 1(a) and (c)) clearly indicates that raw chitosan particles are irregular in shape and PSCCB are slightly spherical in shape. Moreover, the diameter of PSCCB is around 1 µm. When comparing Fig. 1(b) and (d), it is evident that void sizes and the number of voids per unit area in PSCCB are higher than raw chitosan powder. Therefore, PSCCB may provide a higher number of adsorption sites for the adsorption process (Wang et al., 2020).

The surface chemical composition of raw chitosan and PSCCB was obtained from the EDX analysis. Carbon, oxygen and nitrogen content of raw chitosan by weight were 43.66%, 41.82% and 14.52% respectively, and the carbon, oxygen and chlorine content in PSCCB by weight were 56.90%, 38.76% and 4.35% respectively. From the results, it is evident that the nitrogen compounds have been removed and chlorine compounds have been added during the modification process. The addition of chlorine compounds into the PSCCB could be the result of protonating chitosan beads by HCl. Lawrie et al. (2007) reported similar results and also revealed that the percent of chloride is equal to the percent of protonated amines.

3.1.3. Fourier transform infrared spectroscopy (FTIR) analysis

The FTIR spectra of raw chitosan and PSCCB are given in supplementary material. In case of raw chitosan, a broader adsorption band could be observed at 3000–3500 cm⁻¹ wave number region due to the stretching vibration of –OH and –NH₂ functional groups. Even though, the two bands of –OH and –NH₂ have separate peaks they could overlap due to hydrogen bonds and moisture in the chitosan sample thus a broader peak is observed in the same wavelength region (Kasaai, 2008). The C–H stretching band is observed around 2870 cm⁻¹ (Kaczmarek and Zawadzki, 2010). The two peaks occurring at 1645 cm⁻¹ and 1583 cm⁻¹ could be attributed to C=O stretching of amide I and angular deformation of N–H bond in the amine respectively (Corazzari et al., 2015; Kolhe and Kannan, 2003). The three distinct peaks at 1151 cm⁻¹, 1062 cm⁻¹ and 1025 cm⁻¹ were assigned to anti-symmetric stretching of C–O–C and the skeletal vibrations involving the C–O and C–O–C stretching respectively (Cole et al., 2019; Corazzari et al., 2015; Kasaai, 2008). The sharp band at 1375 cm⁻¹ was assigned to –CH₃ symmetric deformation (Corazzari et al., 2015).

A noticeable change in the FTIR spectra of PSCCB is seen in the 800–1700 cm⁻¹ region. The shift of two peaks observed at 1645 cm⁻¹ and 1583 cm⁻¹ of raw chitosan to 1628 cm⁻¹ and 1554 cm⁻¹ confirms successful crosslinking of chitosan with glutaraldehyde occurred at amino groups. Jeon and Höll (2003) also observed a clear peak in 1600–1650 cm⁻¹ region which represented the carbonyl group in glutaraldehyde and it agrees with the above finding. Even though, FTIR plot cannot be used to find the extent of protonation it can be used to identify presence of protonated amine groups in PSCCB. The two bands occurring at 1625–1630 cm⁻¹ range and 1530–1550 cm⁻¹ range could be assigned to antisymmetric and symmetric vibration of –NH₃⁺ respectively. This agrees with the findings of Lawrie et al. (2007) in their study of chitosan biopolymer.

3.1.4. Brunauer-Emmett-Teller (BET) analysis

Specific surface area, pore volume and pore radius data were obtained from the BET analysis for both raw chitosan and PSCCB. BET surface area, BJH pore volume and BJH pore radius of PSCCB were 57.970 m²/g, 0.063 cm³/g and 1.7188 nm respectively and for raw chitosan results were 49.781 m²/g, 0.049 cm³/g and 1.5383 nm respectively. The specific area of PSCCB was increased by 16.45% after modification. Moreover, PSCCB shows a higher pore volume and pore radius compared to raw chitosan.

When compared with the BET surface areas of chitosan composites from previous studies used for fluoride removal, PSCCB possesses a

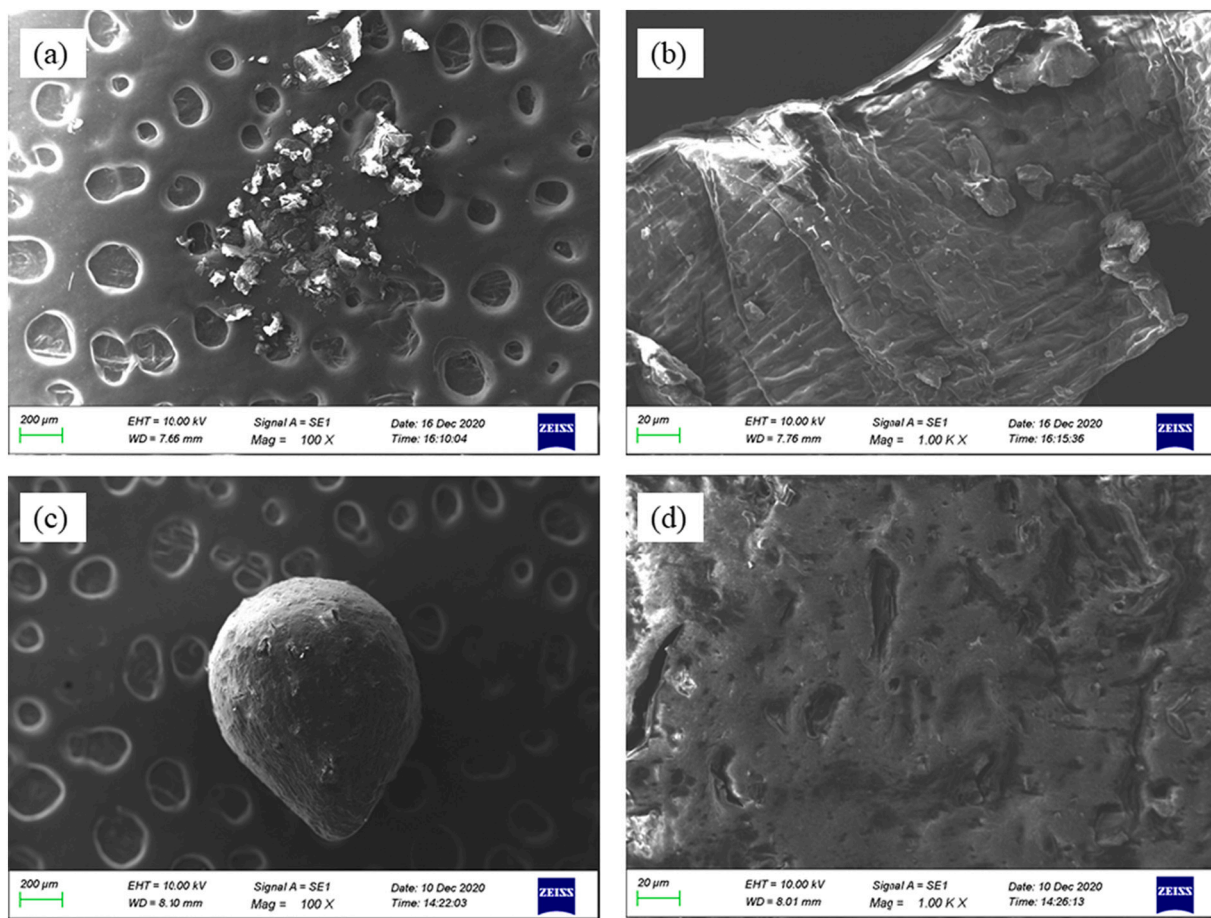


Fig. 1. SEM images of (a) raw chitosan powder — 100 \times , (b) raw chitosan powder — 1000 \times , (c) PSCCB — 100 \times , (d) PSCCB — 1000 \times .

comparatively higher surface area (Huang et al., 2012; Sundaram et al., 2009; Viswanathan et al., 2009a; Viswanathan and Meenakshi, 2008, 2010). Thus, PSCCB facilitates fluoride with a large number of adsorption sites in the adsorption process.

3.1.5. Zero point charge

The pH_{zpc} of raw chitosan powder was found to be at pH 7 whereas, pH_{zpc} of PSCCB was shifted to pH 2.2. Therefore, there was no surface charge in the raw chitosan at neutral pH, suggesting that the raw chitosan may not be able to effectively remove negatively charged fluoride at neutral pH. However, with pH_{zpc} being 2.2 for PSCCB, its surface gets negatively charged at neutral pH. The shifting of pH_{zpc} of PSCCB indicates that the surface structure of the material has been changed (Sundaram et al., 2009). This also suggests that there will be electrostatic repulsive forces between PSCCB surface and negatively charged fluoride ions.

3.2. Sorption studies

3.2.1. Effect of contact time

Fig. 2a shows the variation of fluoride removal with contact time for both raw and PSCCB using an initial fluoride concentration of 5 mg/l with initial pH 7 at room temperature (25 °C). Rapid fluoride adsorption was observed initially for PSCCB and thereafter reaching the equilibrium. PSCCB attained equilibrium at around 60 min while raw chitosan reached equilibrium at around 120 min. This equilibrium time was fixed as contact time for both raw and PSCCB for further experiments. PSCCB showed a very high removal efficiency of more than 90% at equilibrium, whereas only 16% of maximum removal efficiency was observed for raw chitosan at the time of equilibrium.

The rapid uptake of fluoride may be due to the presence of a high concentration gradient between the bulk solution and the adsorbent surface coupled with the availability of highly active sites. Geethamani et al. (2014) observed similar behaviour with their adsorbent and it could be explained as adsorption taking place on the outer surface first, and subsequently, inside the pores. As time elapses, the fluoride concentration in the solution gets reduced, thus reducing the concentration gradient between the bulk solution and the adsorbent surface and thereby reducing the net driving force to overcome the resistance between bulk solution and adsorbent surface (Anbia and Salehi, 2012). Hence the rate of adsorption gradually declines with the attainment of saturation of active sites and functional groups.

3.2.2. Effect of adsorbent dosage

Fig. 2b illustrates the results obtained for the adsorbent dosage study conducted for both raw and PSCCB. The study was conducted with an initial fluoride concentration of 10 mg/l for a dosage ranging from 0.5 g/l to 5 g/l at initial pH of 7 in room temperature (25 °C). For both raw and PSCCB the adsorption capacity decreases with the increase in adsorbent dosage while fluoride removal efficiency increases in PSCCB. The increase in removal efficiency in PSCCB can be attributed to the availability of active sites and increased surface area. When dosage increases from 0.5 g/l to 5 g/l and there is a decrease in the efficiency for raw chitosan. This can be explained due to the agglomeration of chitosan powder, thus decreasing the active surface area and active sites available for adsorption (Padmavathy et al., 2016). The decrease in adsorption capacity could be due to the presence of unsaturated sites during the adsorption process as the initial fluoride concentration is kept constant. (Anbia and Salehi, 2012).

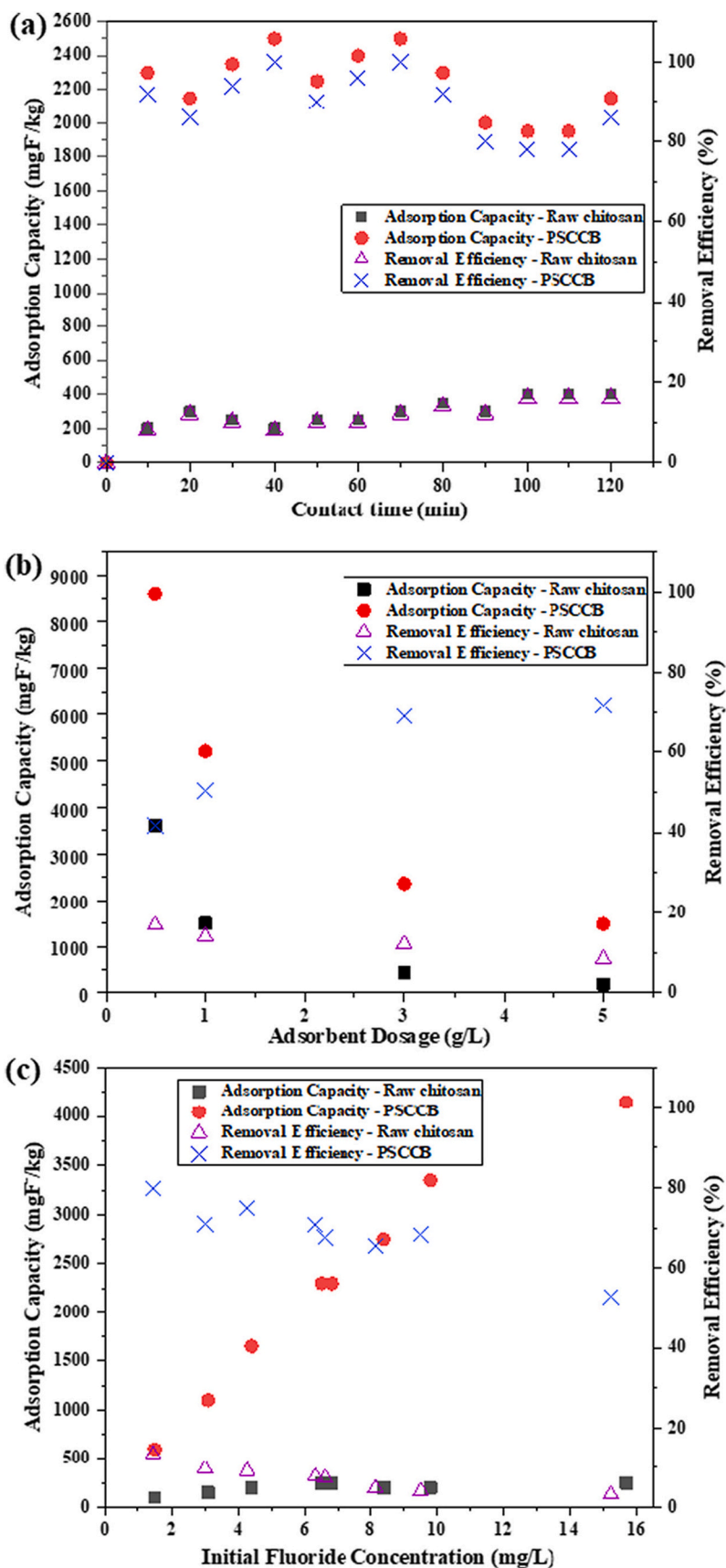


Fig. 2. Adsorption capacity and removal efficiency of PSCCB and raw chitosan as a function of (a) contact time, (b) adsorbent dosage, (c) initial fluoride concentration (temperature = 25 °C; pH = 7).

3.2.3. Effect of initial fluoride concentration

The effect of initial fluoride concentration on adsorption capacities of raw chitosan and PSCCB was investigated with fluoride concentration ranging from 2 mg/l to 15 mg/l for a fixed contact time and the result obtained is illustrated in Fig. 2c. The adsorption capacity of PSCCB increased notably with increase in initial fluoride concentration. This could be due to the fact that at higher fluoride concentrations there is a high concentration gradient acting as a driving force to overcome mass transfer resistance between bulk solution and adsorbent surface (Geethamani et al., 2014; Mann and Mandal, 2014). A significant change of adsorption capacity was not found for raw chitosan. This could be a result of fluoride ions not being able to come in contact with active sites of the raw adsorbent. The decrease in fluoride removal efficiency was observed in both cases since there is a limited number of active sites to accommodate fluoride ions for a certain amount of adsorbent dosage (Patnaik et al., 2016; Yadav et al., 2013).

3.3. Sorption Kinetic Studies

Two of the reaction based kinetic models, pseudo first-order model and pseudo second-order model were employed to the kinetic analysis of fluoride adsorption onto PSCCB. Contact time data reveals that initially, there is rapid uptake of fluoride and thereafter the equilibrium is reached.

3.3.1. Pseudo first order kinetics

Pseudo first order kinetic equation is expressed as;

$$\ln(q_e - q_t) = \ln q_e - k_1 t \quad (1)$$

the linear plot of $\log(q_e - q_t)$ against t yields a straight line. The value of correlation coefficient and k_1 is computed from this plot through linear regression and results are tabulated in Table 2. (q_t is the amount of fluoride on the surface of the sorbent at time t and k_1 is the equilibrium rate constant of pseudo first-order adsorption.)

3.3.2. Pseudo second order kinetics

Pseudo second order kinetic equation is expressed as;

$$\frac{t}{q_t} = \frac{1}{k_2 q_e^2} + \frac{1}{q_e} t \quad (2)$$

the linear plot of t/q_t against t gives a straight line. The values of correlation coefficient and k_2 is computed from this plot through linear regression and results are tabulated in Table 2. (t is the contact time between adsorbate and adsorbent (min), q_t and q_e are the contents of adsorbate removed by an adsorbent at an arbitrary time t and at equilibrium (mg/g), respectively, and k is the rate constant (g/mg min).

The results shown in Table 2 indicate that pseudo second order model is more applicable to the adsorption process. This suggests that the adsorption process is controlled by chemisorption (Wang et al., 2009; Xu et al., 2011). According to Pseudo second order model adsorption capacity at equilibrium is 2409 mg F⁻/kg and the rate constant of pseudo second order adsorption is 0.4157 g/mg min. It could be noted that PSCCB shows high adsorption capacity even at a low initial

Table 2
Kinetics and isotherm model parameters for fluoride removal by PSCCB.

Kinetic/isotherm model	Parameter	R ²
Pseudo first order	$q_e = 0.841$ mg/g $k_1 = 0.0291$ min ⁻¹	0.3096
Pseudo second order	$q_e = 2.409$ mg/g $k_2 = 0.4157$ g/mg min	0.9913
Langmuir isotherm	$q_m = 4.413$ mg/g $k_a = 0.5076$ L/mg	0.9709
Freundlich isotherm	$k_f = 1.355$ (mg/g) (L/mg) ^{1/n} $n = 1.573$	0.9644

fluoride concentration level (5 mg/l), when compared with similar studies (Sundaram et al., 2009; Viswanathan et al., 2009a, 2009b).

3.4. Sorption isotherm studies

Langmuir and Freundlich isotherms were used to predict the maximum adsorption capacity and as well as to identify the adsorbate adsorbent interaction of PSCCB.

The Langmuir isotherm is based on the assumption that the adsorption process is monolayer and adsorption occurs at homogeneous sites with an equal affinity towards adsorbate. The Freundlich isotherm assumes that the adsorption process takes place on heterogeneous surfaces by multilayer adsorption where binding sites have a varying affinity towards adsorbate.

According to the linear form of Langmuir equation:

$$\frac{1}{q_e} = \frac{1}{q_m} + \frac{1}{q_m k_a} \frac{1}{C_e} \quad (3)$$

the plot of $1/q_e$ against $1/C_e$ yields a straight line. C_e (mg/l) is the equilibrium fluoride concentration in solution, q_e (mg/g) is the fluoride concentration in the adsorbent, q_m is the maximum monolayer adsorption capacity of the adsorbent. K_a is the Langmuir equilibrium sorption constant. Constraints obtained from slope and intercept of the linear regression plot of experimental data are summarized in Table 2.

According to the linear form of Freundlich equation:

$$\log q_e = \log k_f + \frac{\log C_e}{n} \quad (4)$$

the plot of $\log q_e$ against $\log C_e$ yields a straight line. The constant k_f is a measure of adsorption capacity and n is a measure of the degree of favorability of the adsorption. Constraints obtained from slope and intercept of the linear regression plot of experimental data are summarized in Table 2.

From the results tabulated in Table 2, the highest correlation coefficient is recorded for Langmuir isotherm which confirms the applicability of the Langmuir isotherm model for the removal of fluoride by PSCCB, indicating monolayer formation of fluoride on the adsorbent surface. According to Langmuir isotherm, the maximum monolayer adsorption capacity is 4413 mg F⁻/kg.

3.4.1. Comparison of adsorption capacities of various adsorbents for fluoride removal

From the comparison of adsorption capacities of various chitosan composites in the literature listed in Table 3, it could be concluded that PSCCB has performed comparatively well in defluoridation. According to Table 3, chitosan beads, when incorporated with metal ions, show relatively higher adsorption since they bind fluoride by chelation. According to the current study the same level of adsorption capacity cannot

Table 3
Adsorption capacities by various adsorbents for fluoride removal.

Adsorbent	q_{max} (mg/g)	Reference
Rice husk-derived biochar	1.856	(Yadav and Jagadevan, 2021)
Chitosan/bentonite composite	2.952	(Liu et al., 2013a)
Protonated chitosan beads	7.32	(Viswanathan et al., 2009a)
Zr(IV) impregnated dithiocarbamate modified chitosan beads	7.782	(Liu et al., 2013b)
Protonated crosslinked chitosan particles	8.10	(Huang et al., 2012)
Al ₂ O ₃ nanoparticles	13.7	(Hafshejani et al., 2017)
Chitosan-ZrO ₂ -Fe ₃ O ₄ composite	17.81	(Korde et al., 2020)
Chitosan/aluminum hydroxide bead	23.06	(Hu et al., 2018)
PSCCB	4.413	Present study

be obtained with incorporation of biochar with chitosan. Moreover, PSCCB in the present study has a lower adsorption capacity compared to protonated beads, where the adsorption capacity was reported as 7.32 mg/g by Viswanathan et al. (2009a) and 8.10 mg/g by Huang et al. (2012) in the literature. The reason behind this could be drawn from the zero point charge characterization in PSCCB. The pH_{zpc} of PSCCB revealed that at neutral pH, the surface gets negatively charged and due to this there exist an electrostatic repulsion between fluoride and PSCCB surface. Even though, an abundant of adsorption sites were available owing to a very high surface area of PSCCB, negatively charged fluoride ions are unable to actively bind to these sites due to these repulsive forces, which has prevented PSCCB from being fully effective at neutral pH.

3.5. Intra particle diffusion model

The kinetic data were further analyzed through intra particle diffusion model which is expressed in Eq. (5)

$$q_t = k_{id} t^{0.5} + B \quad (5)$$

where q_t is the amount of fluoride adsorbed at time t in mg/g, k_{id} is the initial rate of intra particular diffusion ($mg/l \text{ min}^{-1/2}$) and B is the constant related to thickness and mass transfer across the boundary layer. As given in supplementary material, the plot of $t^{0.5}$ vs q_t does not yield a straight line over the whole time but rather it is multi linear. The data is represented by two linear segments which best fit the data. If the plot was passing through zero, the intra particle diffusion might have played a significant role in the adsorption process but based on present data it is implied that more than one mechanism along with intraparticle diffusion is involved in the adsorption process (Chatterjee and Woo, 2009; Geethamani et al., 2014). It could be concluded that adsorption process begins with surface adsorption, represented by first linear portion, followed by intraparticle diffusion of adsorbate into pores, which is the rate limiting step.

3.6. Proposed adsorption mechanisms of fluoride removal

The characterization of PSCCB gives more insight into possible mechanisms occurring simultaneously during adsorption. Besides, the rapid initial adsorption of fluoride onto PSCCB indicates the presence of a high density of active sites on PSCCB. Though the effect of solution pH was not investigated in this study, the removal mechanisms with varying pH could be predicted supported by previous similar studies.

- I. The FTIR analysis confirmed the presence of protonated amines in PSCCB. The results obtained from isotherm studies and kinetic studies reveal that the adsorption process is governed by chemisorption. Hence, for near neutral pH or below, we could propose that the adsorption process of fluoride onto PSCCB might be achieved by the electrostatic interaction of protonated amines with fluoride via hydrogen bonding. This could be proposed as the dominant removal mechanism for fluoride by PSCCB. This is also confirmed by FTIR studies in similar cases in the literature (Huang et al., 2012; Shen et al., 2016; Viswanathan et al., 2009a).
- II. As suggested by the intraparticle diffusion model, since more than one mechanism is involved in the adsorption process, we could suggest that initially, the electrostatic attraction between protonated amines and fluoride could act as a driving force that initiates the adsorption process. Thereafter, fluoride might diffuse into pores and get adsorbed inside the pores since the pore radius of PSCCB (1.7188 nm) is several times greater than the radius of the fluoride ion (0.136 nm). At the same time, having a negatively charged surface for PSCCB at neutral pH ($pH_{zpc} < pH$ 7) could impede fluoride penetrating inside the pores.

- III. EDX analysis confirmed the presence of chloride which exist as the counterion ion of protonated amines; hence, the ion exchange between chloride and more electronegative fluoride might occur in the adsorption process. It should also be noted that fluoride adsorption would be effective over a wide pH range: acidic or alkaline, since anion exchange could occur even when there is an electrostatic repulsion ($pH > pH_{zpc}$) between PSCCB surface and fluoride (Wang et al., 2018).
- IV. BET analysis confirmed a high surface area and pore volume in PSCCB, a property added by biochar which act as a supporting porous material in PSCCB. This is well depicted in the SEM images of PSCCB which shows the appearance of honeycomb like structure. This implies that pore filling effect might contribute in the adsorption of fluoride. This is much likely to happen in acidic conditions due to presence of electrostatic attraction from protonated amines. However, at alkaline conditions OH^- ions compete with F^- ions (since OH^- ionic radius is similar to F^- ionic radius) and might interfere with the adsorption of F^- on to pores (Wan et al., 2019; Wang et al., 2018).
- V. Biochar which acts as a supporting material in PSCCB, is rich with oxygen containing functional groups ($-OH$), as also confirmed by FTIR. Hence, for pH near pH_{zpc} or below, the formation of hydrogen bonds with these functional groups could also be proposed as a possible fluoride removal mechanism, as suggested by several other literatures (Barquilha and Braga, 2021; Li et al., 2019).

Through characterization and mechanism study, it is evident that PSCCB performs exceptionally well in defluoridation due to its superior qualities such as high pore volume and surface area and abundance of functional groups compared to raw chitosan. Fig. 3 shows the proposed adsorption mechanism of fluoride by PSCCB.

3.7. Field observations

Fluoride removal efficiencies of actual ground water sample 1, sample 2 and sample 3 were 66.67%, 15.15% and 60% respectively. It is evident from the results that removal efficiencies are low in the actual ground water samples compared to the synthetic fluoride samples. This may be due to the presence of competitive ions in the actual ground water. Sample 2 which has the highest initial F^- concentration showed the lowest fluoride removal efficiency, due to high level of Na^+ , Mg^{2+} , hardness and TDS present in the sample compared to other two samples. Moreover, PSCCB may have adsorbed cations in groundwater due to its negatively charged surface during the neutral pH condition. This in turn might have hindered the adsorption of negatively charged fluoride.

3.8. Recommendations for future research work

In this study, defluoridation capacity of PSCCB was compared against raw chitosan using synthetic fluoride solutions at neutral pH. The following recommendations are suggested to further explore the capacity and applicability of PSCCB as a biosorbent in defluoridation.

- I. The biochar used in PSCCB was pyrolyzed at 550 °C–660 °C temperature range. Hence, the study of the adsorption capacity of PSCCB with biochar prepared with various pyrolysis temperatures can be suggested to further investigate the adsorption capacity of PSCCB.
- II. High adsorption capacity and better reusability give an important value to the adsorbent. Since crosslinking of PSCCB offers better physical and chemical stability to the bead, it is possible to regenerate the adsorbent using HCL, H_2SO_4 , or NaOH. Hence, a study on the reusability by monitoring the defluoridation efficiency after each recycle step could be suggested to confirm the applicability of the PSCCB in defluoridation.

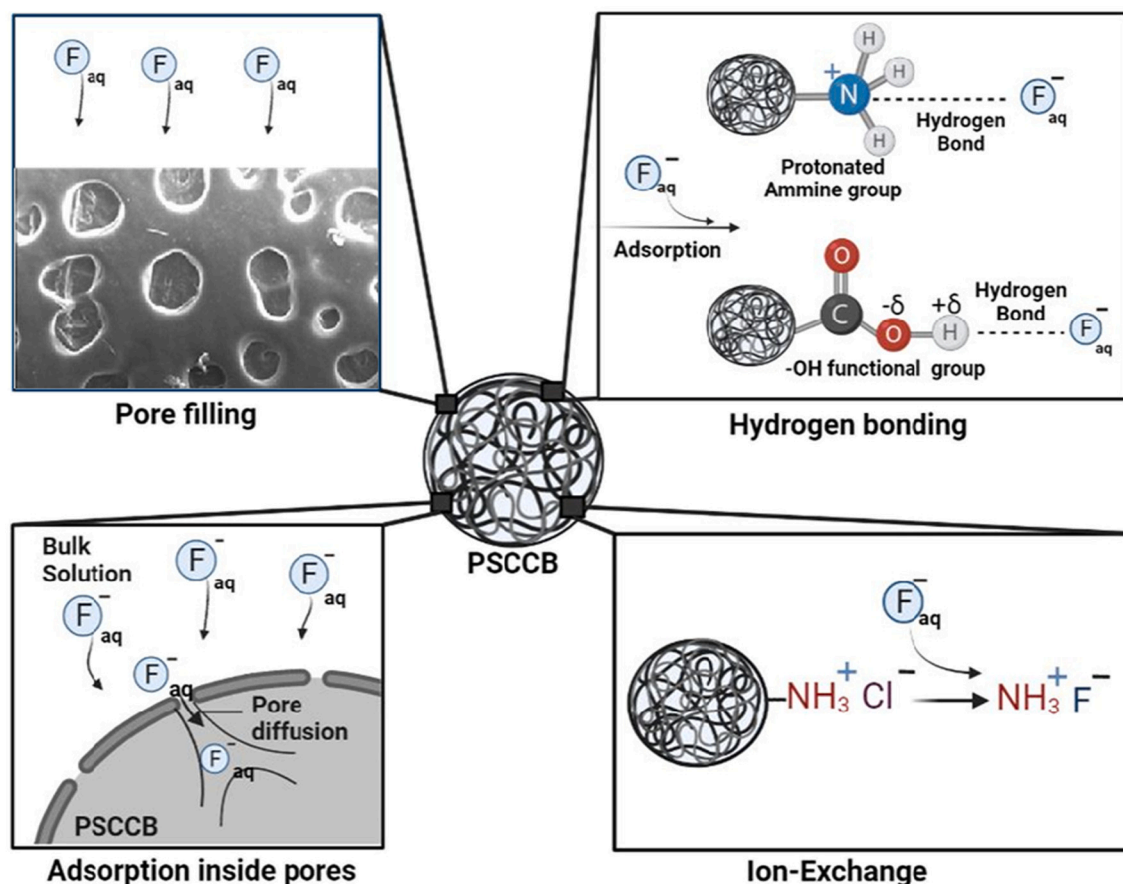


Fig. 3. Proposed adsorption mechanisms of fluoride by PSCCB.

4. Conclusions

PSCCB possesses an excellent defluoridation capacity compared to raw chitosan with more than 90% fluoride removal within 60 min at neutral pH. 16.45% and 28.57% increase in surface area and pore volume, and an increased surface functionality was observed after modification in PSCCB. Langmuir isotherm model and pseudo-second-order kinetic model were fitted well with the experimental data suggesting chemisorption governed adsorption and indicated a maximum monolayer adsorption capacity of 4413 mg F⁻/kg. The formation of hydrogen bonds with protonated amines was proposed as the dominant removal mechanism. Field trial results indicated that the PSCCB could be effective for fluoride removal.

CRedit authorship contribution statement

Nadu Kankanamge Lahiru Chathushan Rupasinghe: Investigation, Formal analysis, Writing – original draft. **Senanayake Mudiyan-selage Aroshi Erandika Senanayake:** Investigation, Formal analysis, Writing – original draft. **K.G.N. Nanayakkara:** Conceptualization, Formal analysis, Supervision, Writing – review & editing, Project administration, Funding acquisition.

Declaration of competing interest

The authors declare that they have no known competing financial interests or personal relationships that could have appeared to influence the work reported in this paper.

Acknowledgements

Authors acknowledge the financial support received from the NORAD Waso-Asia project and the Tokyo Cement Company (Lanka) PLC. Chitosan material from the Norwegian University of Life Sciences also acknowledged.

References

- Anbia, M., Salehi, S., 2012. Removal of acid dyes from aqueous media by adsorption onto amino-functionalized nanoporous silica SBA-3. *Dyes Pigments* 94, 1–9. <https://doi.org/10.1016/j.dyepig.2011.10.016>.
- Ayub, A., Raza, Z.A., Majeed, M.I., Tariq, M.R., Irfan, A., 2020. Development of sustainable magnetic chitosan biosorbent beads for kinetic remediation of arsenic contaminated water. *Int. J. Biol. Macromol.* 163, 603–617. <https://doi.org/10.1016/j.ijbiomac.2020.06.287>.
- Banerjee, A., Singh, A., Roychoudhury, A., 2021. Fluoride toxicity variably affects overall physiology and grain development in three contrasting rice genotypes, representing a potential biohazard. *Environ. Sci. Pollut. Res.* 28, 40220–40232. <https://doi.org/10.1007/s11356-020-10604-7>.
- Barquilha, C.E.R., Braga, M.C.B., 2021. Adsorption of organic and inorganic pollutants onto biochars: challenges, operating conditions, and mechanisms. *Bioresour. Technol. Rep.*, 100728 <https://doi.org/10.1016/j.biteb.2021.100728>.
- Chatterjee, S., Woo, S.H., 2009. The removal of nitrate from aqueous solutions by chitosan hydrogel beads. *J. Hazard. Mater.* 164, 1012–1018. <https://doi.org/10.1016/j.jhazmat.2008.09.001>.
- Cheng, S., Liu, Y., Xing, B., Qin, X., Zhang, C., Xia, H., 2021. Lead and cadmium clean removal from wastewater by sustainable biochar derived from poplar saw dust. *J. Clean. Prod.*, 128074 <https://doi.org/10.1016/j.jclepro.2021.128074>.
- Cole, E.J., Zandvakili, O.R., Xing, B., Hashemi, M., Herbert, S., Mashayekhi, H.H., 2019. Dataset on the effect of hardwood biochar on soil gravimetric moisture content and nitrate dynamics at different soil depths with FTIR analysis of fresh and aged biochar. *Data Brief* 25, 104073. <https://doi.org/10.1016/j.dib.2019.104073>.
- Connor, R., 2015. *The United Nations World Water Development Report 2015: Water for a Sustainable World*. UNESCO Publishing.
- Corazzari, I., Nisticò, R., Turci, F., Faga, M.G., Franzoso, F., Tabasso, S., Magnacca, G., 2015. Advanced physico-chemical characterization of chitosan by means of TGA coupled on-line with FTIR and GCMS: thermal degradation and water adsorption

- capacity. *Polym. Degrad. Stab.* 112, 1–9. <https://doi.org/10.1016/j.polyimdegradstab.2014.12.006>.
- Dai, Y., Zhang, N., Xing, C., Cui, Q., Sun, Q., 2019. The adsorption, regeneration and engineering applications of biochar for removal organic pollutants: a review. *Chemosphere* 223, 12–27. <https://doi.org/10.1016/j.chemosphere.2019.01.161>.
- Dissanayake, C.B., 2010. Water quality in the dry zone of Sri Lanka-some interesting health aspects. In: *J.Natl. Sci.Found.Sri Lanka. J. Natl. Sci. Found. Sri Lanka*, 33.
- Geethamani, C.K., Ramesh, S.T., Gandhimathi, R., Nidheesh, P.v., 2014. Alkali-treated fly ash for the removal of fluoride from aqueous solutions. *Desalination Water Treat.* 52, 3466–3476. <https://doi.org/10.1080/19443994.2013.800825>.
- Guan, X., Zhou, J., Ma, N., Chen, X., Gao, J., Zhang, R., 2015. Studies on modified conditions of biochar and the mechanism for fluoride removal. *Desalin. Water Treat.* 55, 440–447. <https://doi.org/10.1080/19443994.2014.916230>.
- Habuda-Stanić, M., Ravančić, M.E., Flanagan, A., 2014. A review on adsorption of fluoride from aqueous solution. *Materials* 7, 6317–6366. <https://doi.org/10.3390/ma7096317>.
- Hafshejani, L.D., Tangsir, S., Daneshvar, E., Maljanen, M., Lähde, A., Jokiniemi, J., Naushad, Mu., Bhatnagar, A., 2017. Optimization of fluoride removal from aqueous solution by Al₂O₃ nanoparticles. *J. Mol. Liq.* 238, 254–262. <https://doi.org/10.1016/j.molliq.2017.04.104>.
- Hu, H., Yang, L., Lin, Z., Zhao, Y., Jiang, X., Hou, L., 2018. A low-cost and environment friendly chitosan/aluminum hydroxide adsorbent for fluoride removal from aqueous solutions. *Iran. Polym. J.* 27, 253–261. <https://doi.org/10.1007/s13726-018-0605-x>.
- Hu, Huawen, Xin, J.H., Hu, Hong, Chan, A., He, L., 2013. Glutaraldehyde–chitosan and poly (vinyl alcohol) blends, and fluorescence of their nano-silica composite films. *Carbohydr. Polym.* 91, 305–313. <https://doi.org/10.1016/j.carbpol.2012.08.038>.
- Huang, R., Yang, B., Liu, Q., Ding, K., 2012. Removal of fluoride ions from aqueous solutions using protonated cross-linked chitosan particles. *J. Fluor. Chem.* 141, 29–34. <https://doi.org/10.1016/j.jfluchem.2012.05.022>.
- Jeon, C., Höll, W.H., 2003. Chemical modification of chitosan and equilibrium study for mercury ion removal. *Water Res.* 37, 4770–4780. [https://doi.org/10.1016/S0043-1354\(03\)00431-7](https://doi.org/10.1016/S0043-1354(03)00431-7).
- Kaczmarek, H., Zawadzki, J., 2010. Chitosan pyrolysis and adsorption properties of chitosan and its carbonizate. *Carbohydr. Res.* 345, 941–947. <https://doi.org/10.1016/j.carres.2010.02.024>.
- Kasaai, M.R., 2008. A review of several reported procedures to determine the degree of N-acetylation for chitin and chitosan using infrared spectroscopy. *Carbohydr. Polym.* 71, 497–508. <https://doi.org/10.1016/j.carbpol.2007.07.009>.
- Kolhe, P., Kannan, R.M., 2003. Improvement in ductility of chitosan through blending and copolymerization with PEG: FTIR investigation of molecular interactions. *Biomacromolecules* 4, 173–180. <https://doi.org/10.1021/bm025689+>.
- Korde, S., Tandekar, S., Jugade, R.M., 2020. Novel mesoporous chitosan-zirconia-ferrosoferic oxide as magnetic composite for defluoridation of water. *J. Environ. Chem. Eng.* 8, 104360. <https://doi.org/10.1016/j.jece.2020.104360>.
- Kusrini, E., Paramesti, S.N., Zulys, A., Daud, N.Z.A., Usman, A., Wilson, L.D., Sofyan, N., 2019. Kinetics, isotherm, thermodynamic and bioperformance of defluoridation of water using praseodymium-modified chitosan. *J. Environ. Chem. Eng.* 7, 103498. <https://doi.org/10.1016/j.jece.2019.103498>.
- Kut, K.M.K., Sarswat, A., Srivastava, A., Pittman, C.U., Mohan, D., 2016. A review of fluoride in African groundwater and local remediation methods. *Groundw. Sustain. Dev.* 2–3, 190–212. <https://doi.org/10.1016/j.gsd.2016.09.001>.
- Lawrie, K., Keen, I., Drew, B., Chandler-Temple, A., Rintoul, L., Fredericks, P., Grøndahl, L., 2007. Interactions between alginate and chitosan biopolymers characterized using FTIR and XPS. *Biomacromolecules* 8, 2533–2541. <https://doi.org/10.1021/bm070014y>.
- Lee, H.C., Jeong, Y.G., Min, B.G., Lyoo, W.S., Lee, S.C., 2009. Preparation and acid dye adsorption behavior of polyurethane/chitosan composite foams. *Fibers Polym.* 10, 636–642.
- Li, H., Dong, X., da Silva, E.B., de Oliveira, L.M., Chen, Y., Ma, L.Q., 2017. Mechanisms of metal sorption by biochars: biochar characteristics and modifications. *Chemosphere* 178, 466–478.
- Li, X., Wang, C., Zhang, J., Liu, J., Liu, B., Chen, G., 2020. Preparation and application of magnetic biochar in water treatment: a critical review. *Sci. Total Environ.* 711, 134847. <https://doi.org/10.1016/j.scitotenv.2019.134847>.
- Li, X., Zhao, C., Zhang, M., 2019. Biochar for anionic contaminants removal from water. In: *Biochar From Biomass and Waste*. Elsevier, pp. 143–160. <https://doi.org/10.1016/B978-0-12-811729-3.00008-X>.
- Liang, L., Xi, F., Tan, W., Meng, X., Hu, B., Wang, X., 2021. Review of organic and inorganic pollutants removal by biochar and biochar-based composites. *Biochar* 3, 255–281. <https://doi.org/10.1007/s42773-021-00101-6>.
- Liu, B., Wang, D., Yu, G., Meng, X., 2013. Removal of F⁻ from aqueous solution using Zr (IV) impregnated dithiocarbamate modified chitosan beads. *Chem. Eng. J.* 228, 224–231. <https://doi.org/10.1016/j.cej.2013.04.099>.
- Liu, Q., Huang, R., Yang, B., Liu, Y., 2013. Adsorption of fluoride from aqueous solution by enhanced chitosan/bentonite composite. *Water Sci. Technol.* 68, 2074–2081. <https://doi.org/10.2166/wst.2013.456>.
- Liu, R., Wang, H., Han, L., Hu, B., Qiu, M., 2021. Reductive and adsorptive elimination of U(VI) ions in aqueous solution by SFeS@Biochar composites. *Environ. Sci. Pollut. Res.* 28, 55176–55185. <https://doi.org/10.1007/s11356-021-14835-0>.
- Mann, S., Mandal, A., 2014. Removal of fluoride from drinking water using sawdust. *Int. J. Eng. Res. Appl.* 4, 116–123.
- Mohan, D., Sarswat, A., Ok, Y.S., Pittman Jr., C.U., 2014. Organic and inorganic contaminants removal from water with biochar, a renewable, low cost and sustainable adsorbent—a critical review. *Bioresour. Technol.* 160, 191–202. <https://doi.org/10.1016/j.biortech.2014.01.120>.
- Padmavathy, K.S., Madhu, G., Haseena, P.v., 2016. A study on effects of pH, adsorbent dosage, time, initial concentration and adsorption isotherm study for the removal of hexavalent chromium (Cr (VI)) from wastewater by magnetite nanoparticles. *Procedia Technol.* 24, 585–594. <https://doi.org/10.1016/j.protcy.2016.05.127>.
- Patnaik, S., Mishra, P.C., Nayak, R.N., Giri, A.K., 2016. Removal of fluoride from aqueous solution using chitosan-iron complex. *J. Anal. Bioanal. Tech.* 7, 1000326. <https://doi.org/10.4172/2155-9872.1000326>.
- Qiu, M., Hu, B., Chen, Z., Yang, H., Zhuang, L., Wang, X., 2021. Challenges of organic pollutant photocatalysis by biochar-based catalysts. *Biochar* 3, 117–123. <https://doi.org/10.1007/s42773-021-00098-y>.
- Shen, C., Wu, L., Chen, Y., Li, S., Rashid, S., Gao, Y., Liu, J., 2016. Efficient removal of fluoride from drinking water using well-dispersed monetite bundles inlaid in chitosan beads. *Chem. Eng. J.* 303, 391–400. <https://doi.org/10.1016/j.cej.2016.05.103>.
- Strunecka, A., Strunecky, O., 2020. Mechanisms of fluoride toxicity: from enzymes to underlying integrative networks. *Appl. Sci.* 10, 7100. <https://doi.org/10.3390/app10207100>.
- Sundaram, C.S., Viswanathan, N., Meenakshi, S., 2009. Defluoridation of water using magnesium/chitosan composite. *J. Hazard. Mater.* 163, 618–624. <https://doi.org/10.1016/j.jhazmat.2008.07.009>.
- Tomczyk, A., Sokołowska, Z., Boguta, P., 2020. Biochar physicochemical properties: pyrolysis temperature and feedstock kind effects. *Rev. Environ. Sci. Biotechnol.* 19, 191–215. <https://doi.org/10.1007/s11157-020-09523-3>.
- Viswanathan, N., Meenakshi, S., 2010. Enriched fluoride sorption using alumina/chitosan composite. *J. Hazard. Mater.* 178, 226–232. <https://doi.org/10.1016/j.jhazmat.2010.01.067>.
- Viswanathan, N., Meenakshi, S., 2008. Selective sorption of fluoride using Fe (III) loaded carboxylated chitosan beads. *J. Fluor. Chem.* 129, 503–509. <https://doi.org/10.1016/j.jfluchem.2008.03.005>.
- Viswanathan, N., Sundaram, C.S., Meenakshi, S., 2009a. Removal of fluoride from aqueous solution using protonated chitosan beads. *J. Hazard. Mater.* 161, 423–430. <https://doi.org/10.1016/j.jhazmat.2008.03.115>.
- Viswanathan, N., Sundaram, C.S., Meenakshi, S., 2009b. Development of multifunctional chitosan beads for fluoride removal. *J. Hazard. Mater.* 167, 325–331. <https://doi.org/10.1016/j.jhazmat.2008.12.123>.
- Waghmare, S., Arfin, T., Rayalu, S., Lataye, D., Dubey, S., Tiwari, S., 2015. Adsorption behavior of modified zeolite as novel adsorbents for fluoride removal from drinking water: surface phenomena, kinetics and thermodynamics studies. *Int. J. Sci. Eng. Technol. Res.* 4, 4114–4124.
- Wan, S., Lin, J., Tao, W., Yang, Y., Li, Y., He, F., 2019. Enhanced fluoride removal from water by nanoporous biochar-supported magnesium oxide. *Ind. Eng. Chem. Res.* 58, 9988–9996. <https://doi.org/10.1021/acs.iecr.9b01368>.
- Wang, G., Liu, J., Wang, X., Xie, Z., Deng, N., 2009. Adsorption of uranium (VI) from aqueous solution onto cross-linked chitosan. *J. Hazard. Mater.* 168, 1053–1058. <https://doi.org/10.1016/j.jhazmat.2009.02.157>.
- Wang, J., Chen, N., Feng, C., Li, M., 2018. Performance and mechanism of fluoride adsorption from groundwater by lanthanum-modified pomelo peel biochar. *Environ. Sci. Pollut. Res.* 25, 15326–15335. <https://doi.org/10.1007/s11356-018-1727-6>.
- Wang, Z., Zhang, G., Li, Y., 2020. Preparation of chitosan/polyacrylamide/graphene oxide composite membranes and study of their methylene blue adsorption properties. *Materials* 13, 4407. <https://doi.org/10.3390/ma13194407>.
- Wu, L., Du, C., He, J., Yang, Z., Li, H., 2020. Effective adsorption of diclofenac sodium from neutral aqueous solution by low-cost lignite activated cokes. *J. Hazard. Mater.* 384, 121284. <https://doi.org/10.1016/j.jhazmat.2019.121284>.
- Wu, L., Fan, C., Zhang, Z., Zhang, X., Lou, Q., Guo, N., Huang, W., Zhang, M., Yin, F., Guan, Z., Yang, Y., Gao, Y., 2021. Association between fluoride exposure and kidney function in adults: a cross-sectional study based on endemic fluorosis area in China. *Ecotoxicol. Environ. Saf.* 225, 112735. <https://doi.org/10.1016/j.ecoenv.2021.112735>.
- Xu, X., Li, Q., Cui, H., Pang, J., Sun, L., An, H., Zhai, J., 2011. Adsorption of fluoride from aqueous solution on magnesium-loaded fly ash cenospheres. *Desalination* 272, 233–239. <https://doi.org/10.1016/j.desal.2011.01.028>.
- Yadav, A.K., Abbassi, R., Gupta, A., Dadashzadeh, M., 2013. Removal of fluoride from aqueous solution and groundwater by wheat straw, sawdust and activated bagasse carbon of sugarcane. *Ecol. Eng.* 52, 211–218. <https://doi.org/10.1016/j.ecoeng.2012.12.069>.
- Yadav, K., Jagadevan, S., 2021. Effect of pyrolysis of rice husk-derived biochar on the fuel characteristics and adsorption of fluoride from aqueous solution. *BioEnergy Res.* 14, 964–977. <https://doi.org/10.1007/s12155-020-10189-6>.
- Zhang, J., Yu, L., Yang, H., Ye, B.-C., 2018. Migration and transformation of fluoride through fluoride-containing water for the irrigation of a soil–plant system. *Hum. Ecol. Risk Assess. Int. J.* 25, 1048–1058. <https://doi.org/10.1080/10807039.2018.1460577>.
- Zhang, Y., Liu, B.-L., Wang, L.-J., Deng, Y.-H., Zhou, S.-Y., Feng, J.-W., 2019. Preparation, structure and properties of acid aqueous solution plasticized thermoplastic chitosan. *Polymers* 11, 818. <https://doi.org/10.3390/polym11050818>.
- Zhou, Y., Liu, X., Xiang, Y., Wang, P., Zhang, J., Zhang, F., Wei, J., Luo, L., Lei, M., Tang, L., 2017. Modification of biochar derived from sawdust and its application in removal of tetracycline and copper from aqueous solution: adsorption mechanism and modelling. *Bioresour. Technol.* 245, 266–273. <https://doi.org/10.1016/j.biortech.2017.08.178>.